Nonisothermal Photochlorination of Methyl Chloride in the Liquid Phase

María I. Cabrera, Orlando M. Alfano, and Alberto E. Cassano
Instituto de Desarrollo Tecnológico para la Industria Química, Universidad Nacional del Litoral and Consejo Nacional de Investigaciones Científicas y Técnicas, Santa Fe, Argentina

A model for the photochlorination of methyl chloride in the liquid phase was developed, with numerical solution and experimental verification. The reaction was carried out under pressure, using carbon tetrachloride as a solvent with polychromatic radiation in a nonisothermal tubular reactor. Momentum, thermal energy, mass and photon balances were established rigorously and solved numerically. Reaction constants were taken from the known reaction mechanistic kinetics in the gas phase. Theoretical results agreed well with bench-scale experiments performed inside an elliptical reflector in the prediction of both reactant conversion and product selectivities. The validated model was used to show the existence of significant temperature and concentration gradients inside the reactor, both in the radial and in the axial directions.

Introduction

Methane chlorination has been used for many years as the conventional technology for producing most of the methane-chlorinated derivatives, except for carbon tetrachloride. It may use a thermal, catalytic or photochemical method, but the thermal method is used more widely for large-scale processes. The photochlorination of methane in the gas phase has been studied recently from an engineering viewpoint by De Bernardez and Cassano (1986) and Cabrera et al. (1991a,b). In these works, the pertinent literature survey has been presented. Although the photochemical route is recognized to have some advantages, mainly because the low-temperature operating conditions minimize carbon and tar deposition, its applications have been restricted to medium- and small-scale productions (Hirschkind, 1949; McKetta and Cunningham, 1979).

More recently, alternative processes were introduced with important changes in the production concept—improving the process control and safety, and reducing difficulties associated with the separation of hydrochloric acid and each of the chlorinated products. Thus, methyl chloride is obtained by catalytic hydrochlorination of methanol at high temperature. Methyl chloride undergoes successive catalytic chlorinations in the liquid phase, under pressure and moderate temperatures to produce methylene chloride, chloroform, and carbon tetrachloride. Reducing the product output pressure in several stages allows the collection of different product streams, which simplifies further separation procedures and reduces costs (see Tokuyama process in Akiyama et al., 1984).

Methylene chloride is one of the more attractive solvents used in industrial applications because of its low toxicity. Therefore, for the separation process to be cost-effective, there has been an increased demand in the selective production of dichloromethane. A German patent of 1938 suggested the photochlorination of methyl chloride at 253 K (−20°C) with an excess of chloromethane with respect to chlorine in the feed, indicating the minimal formation of tri- and tetraderivatives (Braun et al., 1986). In addition, a Japanese patent filed in 1982 advocated the selective production of dichloromethane to be done by adjusting properly the operating conditions of the photochlorination of methyl chloride (Braun et al., 1986).

The photochlorination of methyl chloride in a perfectly mixed reactor was also patented by Masini (1984), with these operating conditions: temperature between 50 and 120°C, pressure between 1 and 5 MPa, and chlorine to methyl chloride ratio in the feed between 0.3 and 1.5. A more recent patent by Holbrook and Morris (1986) reports a photoprocess using a stirred tank reactor, also in the liquid phase, with pressures between 700 and 5,000 kPa and temperatures between 40 and 175°C. The chlorine is fed into the reactor in liquid form

Correspondence concerning this article should be addressed to A. E. Cassano.

dissolved in carbon tetrachloride or sparged as a gas into the liquid reactant, while the methyl chloride is introduced in liquid form. These two references are important because they indicate the feasibility of designing a photochemical process under pressure.

The difficulties in performing a photoreaction under pressure can be foreseen easily if one considers that under all circumstances, in industrial applications, at least one of the reactor walls (or the lamp jacket) must be made of quartz or glass. In fact, only Boynton et al. (1959) report on an actual process (a sulfochlorination) performed under pressure. It consisted of a spiral-coiled tube, 0.635 cm inside diameter and 6,100 cm long, which was immersed in a boiling, confined hydrocarbon in such a way that the pressure exerted externally counteracted the internal pressure of the reactor tube. The temperatures were between 90 and 105°C, and a pressure of 810 kPa were used in that research. The reacting coil surrounded a series of twelve 400-W lamps, and its production rate was 0.165 m^3/d.

For faster reactions and higher production rates, simpler, continuous, tubular photoreactors could be used under moderate pressures in industrial processes, if a multitube, single-lamp photoreactor is used. Several tubes with a diameter reduced to the point of withstanding the desired pressure, made of glass or quartz, could be arranged to form a pseudo-annular reacting space surrounding a tubular lamp. This arrangement also has more degrees of freedom for satisfying heating and/or cooling requirements. Additionally, it may include a cylindrical reflector of circular cross-section surrounding the tubes. For a simple reaction, this type of reactor configuration has been modeled and verified experimentally (Tymoschuk, 1990).

Photoreactor engineering design methods have been described recently by Cassano et al. (1986), De Bernardez et al. (1987), and Cassano and Alfano (1989). However, no photoreactor modeling with a subsequent experimental verification, for the photochlorination of methane derivatives in the liquid phase and under pressure, has been reported in the literature.

In this work, the photochlorination of methyl chloride in a single liquid phase, employing carbon tetrachloride as a solvent at 450 kPa, is modeled, and its predictions are compared with the experimental data obtained in a bench-scale photoreactor. The reaction was studied under nonisothermal conditions (the air temperature surrounding the reactor equal to 293 K and temperature of the feed equal to 291 K) using polychromatic radiation in a continuous tubular reactor. The bench-scale cylindrical reactor was placed inside an elliptical reflector and was irradiated from outside by means of a tubular lamp with fluorescent emission (superficial emission).

The required kinetic information for the complete reaction mechanism was obtained from a previous work (Cabrera et al., 1991a) on the photochlorination of methane in the gas phase. Carbon tetrachloride is the usual solvent for these reactions and is used to facilitate the reactor control in many industrial operating conditions. Its nonpolar characteristics permit to assume that the kinetic data obtained in the gas phase should also be valid for the liquid-phase operation. This is also a part of the proposed modeling and was verified experimentally.

This article shows good agreement between the model predictions and the experimental data. It also discusses the conditions under which methylene chloride may be produced with high selectivity. An important model prediction indicates the existence of large concentration and temperature gradients both in the radial and axial directions, when the reaction is performed in the liquid phase.

The approach taken allows any change of scale for any desired size or geometry, and better yet, use of these results to optimize any form of reactor and/or process. This extrapolation is possible because the proposed method uses a deterministic approach with no empirically adjusted parameters and no laboratory-dependent kinetic constants. Therefore, the mathematical representation of the system and all the physicochemical data are useful to predict the performance of any industrial-size equipment, such as the multitube reactor *a priori*. Because of the high radiation absorption of liquid chlorine or, alternatively, the high solubility of the chlorine gas in such solvents as carbon tetrachloride (which again means a high radiation absorption), the radiation characteristic dimension of the tubular flow reactors (the diameter) can never be too large, even in a commercial unit.

Table 1. Simplified Reaction Mechanism

Initiation Step	$Cl_2 \xrightarrow{\Phi e^a} 2\ Cl.$	M-1
Propagation Steps		
	$ClCH_3 + Cl. \rightleftharpoons ClCH_2. + ClH$	M-2, M-2′
	$ClCH_2. + Cl_2 \rightleftharpoons Cl_2CH_2 + Cl.$	M-3, M-3′
	$Cl_2CH_2 + Cl. \rightleftharpoons Cl_2CH. + ClH$	M-4, M-4′
	$Cl_2CH. + Cl_2 \rightleftharpoons Cl_3CH + Cl.$	M-5, M-5′
	$Cl_3CH + Cl. \rightleftharpoons Cl_3C. + ClH$	M-6, M-6′
	$Cl_3C. + Cl_2 \rightleftharpoons Cl_4C + Cl.$	M-7, M-7′
Homogeneous Termination Steps		
	$Cl. + ClCH_2. \rightarrow Cl_2CH_2$	M-8
	$Cl. + Cl_2CH. \rightarrow Cl_3CH$	M-9
	$Cl. + Cl_3C. \rightarrow Cl_4C$	M-10
	$Cl. + Cl. + M \rightarrow Cl_2 + M$	M-11

Reaction Kinetics

Reaction mechanism

The complete reaction mechanism for the chlorination of methyl chloride comprises 27 possible steps (De Bernardez and Cassano, 1986). The following simplifications can reduce the working mechanism to 17 steps: 1. negligible reactions at the walls (Calvert and Pitts, 1966; De Bernardez and Cassano, 1986); 2. negligible termination reactions that form ethane chloroderivatives as compared with other termination steps (De Bernardez and Cassano, 1986). It is represented in Table 1. The associated specific rate constants for the simplified reaction mechanism agree within ±5% with the classical fundamental results by Chiltz et al. (1963). Thus, the 17 steps give an almost exact representation of the following global reaction sequence:

$$ClCH_3 + Cl_2 \Leftrightarrow Cl_2CH_2 + ClH \quad (R1)$$

$$Cl_2CH_2 + Cl_2 \Leftrightarrow Cl_3CH + ClH \quad (R2)$$

$$Cl_3CH + Cl_2 \Leftrightarrow Cl_4C + ClH \quad (R3)$$

Stable species reaction rates

The reaction kinetics was formulated following the well-

Table 2. Arrays for the Reaction Rate Expressions

Denomination	Symbol	Definition
Propagation Reaction Array	$\underset{\sim}{A}(\Psi, \underline{K}_p)$	$\begin{bmatrix} -(K_3\Psi_5+K_2'\Psi_6) & 0 & 0 & K_2\Psi_1+K_3'\Psi_2 \\ 0 & -(K_5\Psi_5+K_4'\Psi_6) & 0 & K_4\Psi_2+K_5'\Psi_3 \\ 0 & 0 & -(K_7\Psi_5+K_6'\Psi_6) & K_6\Psi_3+K_7'\Psi_4 \\ K_3\Psi_5+K_2'\Psi_6 & K_5\Psi_5+K_4'\Psi_6 & K_7\Psi_5+K_6'\Psi_6 & -(K_2\Psi_1+K_4\Psi_2+K_6\Psi_3+K_3'\Psi_2+K_5'\Psi_3+K_7'\Psi_4) \end{bmatrix}$
Intermediate Species Concentration Array	$\underset{\sim}{R}(\hat{\Psi})$	$\begin{bmatrix} \hat{\Psi}_1 & 0 & 0 & 0 \\ 0 & \hat{\Psi}_2 & 0 & 0 \\ 0 & 0 & \hat{\Psi}_3 & 0 \\ 0 & 0 & 0 & \hat{\Psi}_5 \end{bmatrix}$
Termination Constant Array	$\underset{\sim}{T}(\underline{K}_t)$	$\begin{bmatrix} 0 & 0 & 0 & K_8 \\ 0 & 0 & 0 & K_9 \\ 0 & 0 & 0 & K_{10} \\ K_8 & K_9 & K_{10} & 2K_{11} \end{bmatrix}$
Initiation Reaction Array	$\underline{g}(\Psi, \underline{x})$	$[0 \quad 0 \quad 0 \quad J]$
Stable Species Reaction Array	$\underset{\sim}{B}(\hat{\Psi}, \underline{K}_p)$	$\begin{bmatrix} -K_2\hat{\Psi}_5 & 0 & 0 & 0 & 0 & K_2'\hat{\Psi}_1 \\ K_2\hat{\Psi}_5 & -K_4\hat{\Psi}_5 & 0 & 0 & 0 & -K_2'\hat{\Psi}_1+K_4'\hat{\Psi}_2 \\ 0 & K_4\hat{\Psi}_5 & -K_6\hat{\Psi}_5 & 0 & 0 & -K_4'\hat{\Psi}_2+K_6'\hat{\Psi}_3 \\ 0 & 0 & K_6\hat{\Psi}_5 & 0 & 0 & -K_6'\hat{\Psi}_3 \\ -K_2\hat{\Psi}_5 & -K_4\hat{\Psi}_5 & -K_6\hat{\Psi}_5 & 0 & 0 & K_2'\hat{\Psi}_1+K_4'\hat{\Psi}_2+K_6'\hat{\Psi}_3 \\ K_2\hat{\Psi}_5 & K_4\hat{\Psi}_5 & K_6\hat{\Psi}_5 & 0 & 0 & -(K_2'\hat{\Psi}_1+K_4'\hat{\Psi}_2+K_6'\hat{\Psi}_3) \end{bmatrix}$

known mass action law. The local or micro steady-state approximation (MSSA) was used for the unstable, intermediate species (atomic chlorine and free radicals). De Bernardez and Cassano (1986) have shown that this approximation can be used safely for the chlorination of methane. The following notation was used for the reacting species:

1	2	3	4	5	6
$ClCH_3$	Cl_2CH_2	Cl_3CH	Cl_4C	Cl_2	ClH
$\hat{1}$	$\hat{2}$	$\hat{3}$		$\hat{5}$	
$ClCH_2.$	$Cl_2CH.$	$Cl_3C.$		Cl.	

With the definitions in Table 2, the reaction rates of the intermediate species can be written in a compact way:

$$\hat{\Omega} = \underset{\sim}{A}(\Psi, \underline{K}_p)\cdot\hat{\Psi} - \underset{\sim}{R}(\hat{\Psi})\cdot\underset{\sim}{T}(\underline{K}_t)\cdot\hat{\Psi} + 2\underline{g}(\Psi, \underline{x}) \tag{1}$$

where the contributions of the propagation, termination and initiation steps are separated. In Eq. 1, $\hat{\Psi}$ is the dimensionless array of intermediate species concentrations, and Ψ is the dimensionless array of stable species concentrations.

After application of the MSSA ($\hat{\Omega} = \underline{0}$), the concentrations of atomic chlorine and free radicals can be obtained from the solution of the following set of algebraic equations:

$$J - (K_8\Psi_{\hat{1}} + K_9\Psi_{\hat{2}} + K_{10}\Psi_{\hat{3}} + K_{11}\Psi_M\Psi_{\hat{5}})\Psi_{\hat{5}} = 0 \tag{2}$$

$$\Psi_{\hat{1}} = \frac{K_2\Psi_1 + K_3'\Psi_2}{K_2'\Psi_6 + K_3\Psi_5 + K_8\Psi_{\hat{5}}}\Psi_{\hat{5}} \tag{3}$$

$$\Psi_{\hat{2}} = \frac{K_4\Psi_2 + K_5'\Psi_3}{K_4'\Psi_6 + K_5\Psi_5 + K_9\Psi_{\hat{5}}}\Psi_{\hat{5}} \tag{4}$$

$$\Psi_{\hat{3}} = \frac{K_6\Psi_3 + K_7'\Psi_4}{K_6'\Psi_6 + K_7\Psi_5 + K_{10}\Psi_{\hat{5}}}\Psi_{\hat{5}} \tag{5}$$

where J is the dimensionless rate of reaction for the initiation step given by:

$$J = \frac{R_{\text{init}}L_R}{\langle v_z\rangle C_5^0} \tag{6}$$

In Eq. 6, the dimensional rate of initiation constitutes the specific characteristic of a photochemical reactor.

If the reaction rate for the stable species is written by using the matrix representation of Table 2, it is possible to obtain:

$$\Omega = \underset{\sim}{B}(\hat{\Psi}, \underline{K}_p).\Psi \tag{7}$$

where $\hat{\Psi}$ is given by Eqs. 2–5, and $\underline{K}_p$ may be calculated from the available kinetic information of the propagation steps.

Rate of initiation

For polychromatic radiation, the initiation rate can be expressed in terms of the integral over all the useful frequencies, of the product of the monochromatic primary quantum yield times the monochromatic value of the local volumetric rate of energy absorption (LVREA). In turn, the LVREA can be given as a function of the incident radiation and the Naperian absorption coefficient (Irazoqui et al., 1976). Thus,

$$R_{\text{init}} = \int_{\nu=0}^{\nu=\infty} \Phi_\nu e_\nu^a \, d\nu = \int_{\nu=0}^{\nu=\infty} \Phi_\nu \mu_\nu G_\nu \, d\nu \tag{8}$$

where the incident radiation is defined as a function of the radiation spectral specific intensity as follows (Özisik, 1973):

$$G_\nu = \int_{4\pi} I_\nu \, d\Omega \tag{9}$$

To evaluate the incident radiation, the equation of radiative transfer must be solved. It requires, in a photochemical reactor, an additional balance (the photon inventory along the trajectory of each radiation bundle).

Reactor Model

As usual, the momentum, mass, thermal and radiation energy balances must be written, each requiring some simplifying assumptions.

Momentum balance

The classical parabolic profile for the cylindrical tube is obtained assuming steady state, incompressible flow of a Newtonian fluid, azimuthal symmetry, fully developed laminar flow, constant physical properties, and velocity profile independent of the mass transfer rates, as well as using the centerline symmetry and the nonslipping boundary conditions. In cylindrical coordinates in dimensionless form, we have:

$$U(\gamma) = 2(1-\gamma^2) \tag{10}$$

Thermal energy balance

Since the reactor will operate under nonisothermal conditions and chlorinations are highly exothermic, the thermal energy balance will be needed. The following additional assumptions are required: negligible thermal effects of the employed radiation; negligible viscous dissipation; negligible axial conduction as compared with the convective flow; and constant temperature for the fluid surrounding the reactor walls. Then, with the usual boundary conditions, the following equations result, in dimensionless form:

$$U(\gamma)\frac{\partial \tau}{\partial \eta} = \frac{1}{Pe_t\, Ge}\frac{1}{\gamma}\frac{\partial}{\partial \gamma}\left(\gamma \frac{\partial \tau}{\partial \gamma}\right) + Q \tag{11}$$

Initial Condition:

$$0 \le \gamma \le 1;\ \eta = 0;\ \tau = 0 \tag{11a}$$

Boundary Condition 1:

$$0 \le \eta \le 1;\ \gamma = 0;\ \frac{\partial \tau}{\partial \gamma} = 0 \tag{11b}$$

Boundary Condition 2:

$$0 \le \eta \le 1;\ \gamma = 1;\ \frac{\partial \tau}{\partial \gamma} + \frac{1}{2}\mathrm{Nu}(\tau - 1) = 0 \tag{11c}$$

The dimensionless velocity profile is obtained from Eq. 10, and the dimensionless heat generation term Q must be obtained from the heats of reaction of each of the three global reactions described by Eqs. R1, R2, and R3 in the following manner:

$$Q = \frac{L_R \sum_{k=1}^{3} (-\Delta H^{(k)}) R^{(k)}}{\rho\, Cp \langle v_z \rangle (T_c - T^0)} \tag{12}$$

Clearly, the thermal energy equation is coupled with the mass balances through this expression for Q, because the heat generation requires the reaction rate at each point inside the reactor.

Mass balances

In theory, one mass balance for each of the species present in the reaction should be required. However, since the MSSA has been applied all the concentrations of the unstable species can be obtained as a function of the concentration of the stable ones. This procedure reduces significantly the number of partial differential equations to be solved.

The following additional simplifying assumptions are made: axial diffusion is negligible compared with the axial convective flow; and Fickian forms for the diffusion coefficients of the multicomponent mixture are used. Since wall (heterogeneous) terminations were neglected, the boundary conditions are reduced to the symmetry condition at the reactor centerline and the nonpermeability of the reactor walls. The resulting equations, in dimensionless form, are:

$$U(\gamma)\frac{\partial \Psi_i}{\partial \eta} = \frac{1}{Pe_i\, Ge}\frac{1}{\gamma}\frac{\partial}{\partial \gamma}\left(\gamma \frac{\partial \Psi_i}{\partial \gamma}\right) + \Omega_i;\ i = 1 \text{ to } 6 \tag{13}$$

Initial Condition:

$$0 \le \gamma \le 1;\ \eta = 0;\ \Psi_i = \Psi_i^0 \tag{13a}$$

Boundary Condition 1:

$$0 \le \eta \le 1;\ \gamma = 0;\ \frac{\partial \Psi_i}{\partial \gamma} = 0 \tag{13b}$$

Boundary Condition 2:

$$0 \le \eta \le 1;\ \gamma = 1;\ \frac{\partial \Psi_i}{\partial \gamma} = 0 \tag{13c}$$

In Eq. 13, $i = 1$ to 6, stands for each of the stable species.

Table3. Reaction Rate Expressions in Terms of the LVREA

Reaction Rates for Stable Species

$$\Omega_1 = -\kappa^{(1)}\Psi_1\Psi_5 J^{1/2}$$

$$\Omega_2 = (\kappa^{(1)}\Psi_1 - \kappa^{(2)}\Psi_2)\Psi_5 J^{1/2}$$

$$\Omega_3 = (\kappa^{(2)}\Psi_2 - \kappa^{(3)}\Psi_3)\Psi_5 J^{1/2}$$

$$\Omega_4 = \kappa^{(3)}\Psi_3\Psi_5 J^{1/2}$$

$$\Omega_5 = -(\kappa^{(1)}\Psi_1 + \kappa^{(2)}\Psi_2 + \kappa^{(3)}\Psi_3)\Psi_5 J^{1/2}$$

$$\Omega_6 = (\kappa^{(1)}\Psi_1 + \kappa^{(2)}\Psi_2 + \kappa^{(3)}\Psi_3)\Psi_5 J^{1/2}$$

Employed Definitions

$$\kappa^{(1)} = K_2\left[\frac{K_8}{\alpha} + \frac{K_9}{\beta} + \frac{K_{10}}{\gamma} + K_{11}\Psi_M\right]^{-1/2}$$

$$\kappa^{(2)} = K_4\left[\frac{K_8}{\alpha} + \frac{K_9}{\beta} + \frac{K_{10}}{\gamma} + K_{11}\Psi_M\right]^{-1/2}$$

$$\kappa^{(3)} = K_6\left[\frac{K_8}{\alpha} + \frac{K_9}{\beta} + \frac{K_{10}}{\gamma} + K_{11}\Psi_M\right]^{-1/2}$$

$$\alpha = \frac{K_3\Psi_5}{K_2\Psi_1};\ \beta = \frac{K_5\Psi_5}{K_4\Psi_2};\ \gamma = \frac{K_7\Psi_5}{K_6\Psi_3}$$

The required reaction rates for the mass balances can be written in a way that makes explicit their functional dependence on the LVREA. This functional dependence can be seen clearly applying an additional assumption: the long-chain approximation in Table 3. The mass balances and, as a direct consequence the thermal energy balance, due to the necessity of evaluating the LVREA, will need the local values of the incident radiation G. Hence, both balances are coupled with the radiative transfer equation. An Arrhenius type temperature dependence for each of the individual reaction rate constants was assumed.

Radiation equation

A complete derivation of the radiative transfer equation for photochemical reactors has been discussed by Santarelli (1983). Proper use of this equation incorporates the point values of G_ν (and after integrating over all useful frequencies, G) into the reaction rate expressions of mass balances. For designing a photoreactor one would like to be able to express the incident radiation among other variables and parameters, in terms of the radiation source properties. To do it, three separate radiation balances must be used:

1. One equation for the source (an emission model for the tubular lamp) that relates its output power, output power spectral distribution, and the physical dimensions of the lamp to the value of the spectral specific intensity emitted by the lamp in every outgoing direction of radiation propagation comprising the solid angle of emission from each point of the source extent.

2. One equation for the space existing between the lamp and the reactor wall to relate for every outgoing direction the value of the spectral specific intensity existing at the lamp to the one at the reactor boundary. If this space is diactinic, both intensities will be equal.

3. One equation inside the reaction space to relate for every incoming direction of radiation energy the value of the spectral specific intensity at the wall to that at every point inside the reactor, accounting for the absorption by the reacting mixture and changes in concentrations inside the reactor.

Combining the three balances, the value of G_ν (and G after integration over the frequency range of interest for polychromatic radiation) inside the reactor can be related to the lamp characteristics previously mentioned.

In 1976, Yokota et al., using an extension of the extense source model with voluminal emission (Irazoqui et al., 1973, Cerdá et al., 1973), proposed a similar formulation for superficial diffuse emission that represents better the characteristics of a fluorescent lamp. Although they used a different reasoning, the result is identical to the one that would be obtained by combination of the three radiation balances described before.

The main assumptions involved in this derivation are: the lamp and the reactor are perfect cylinders; the emission is superficial and diffuse; the emission of each elementary surface of the lamp is proportional to its extent; the emission by the lamp is uniform in all its extent; the space between the lamp and the reactor is diactinic; refraction effects by the reactor walls are neglected; there is no emission inside the reactor (low temperature and no fluorescence phenomena); and no radiation scattering is present.

The used experimental setup consisted of a right cylindrical reflector of elliptical cross-section, with the cylindrical tubular reactor located in one of the ellipse focal axis and the cylindrical tubular radiation source in the other. This particular arrangement, very useful for laboratory and bench-scale work, was proposed first by Baginski (1951). One more assumption is needed: reflection by the elliptical cylinder is of the specular type.

In the elliptical reflector, the reactor can be irradiated by direct and indirect radiation. Cerdá et al. (1973, 1977) have shown that with proper geometrical sizing, only indirect radiation with one reflection will be significant. De Bernardez and Cassano (1982) have shown that there exist additional, specific geometrical relationships that must be fulfilled to have azimuthal symmetry in the radiation field about the reactor centerline. Both requirements have been satisfied in the bench-scale equipment design used in this work.

Combining the results of Yokota et al. (1976) and Cerdá et al. (1977), the following expression for the value of the LVREA, with polychromatic radiation, can be obtained (Cabrera et al., 1991a):

$$e^a = \frac{C_5}{\pi A_L}\int_{\phi_1}^{\phi_2} d\phi\,\frac{(r_L^2 - D^2\sin^2\xi)^{1/2}}{r_L}\int_{\theta_1(\phi)}^{\theta_2(\phi)} d\theta\sin^2\theta\sum_{\Delta j=1}^{n}\Gamma_{Rf,\Delta j}\Upsilon_{R,\Delta j}$$

$$\times\alpha_{\Delta j}E_{\Delta j}\exp\left[-\int_{\rho_0^*(\theta,\,\phi)}^{\rho_1^*(\theta,\,\phi)}(\alpha_{\Delta j}C_5 + \mu_4)d\rho'\right] \qquad (14)$$

The integration limits for Eq. 14, obtained through intricate trigonometric relationships, were presented systematically by Cerdá et al. (1977) and were summarized by Clariá et al. (1988). They will not be repeated here. In Eq. 14, the exponential attenuation integral takes into account that in this reacting system, the solvent (carbon tetrachloride) also absorbs radiation. The polychromatic nature of the employed radiation was

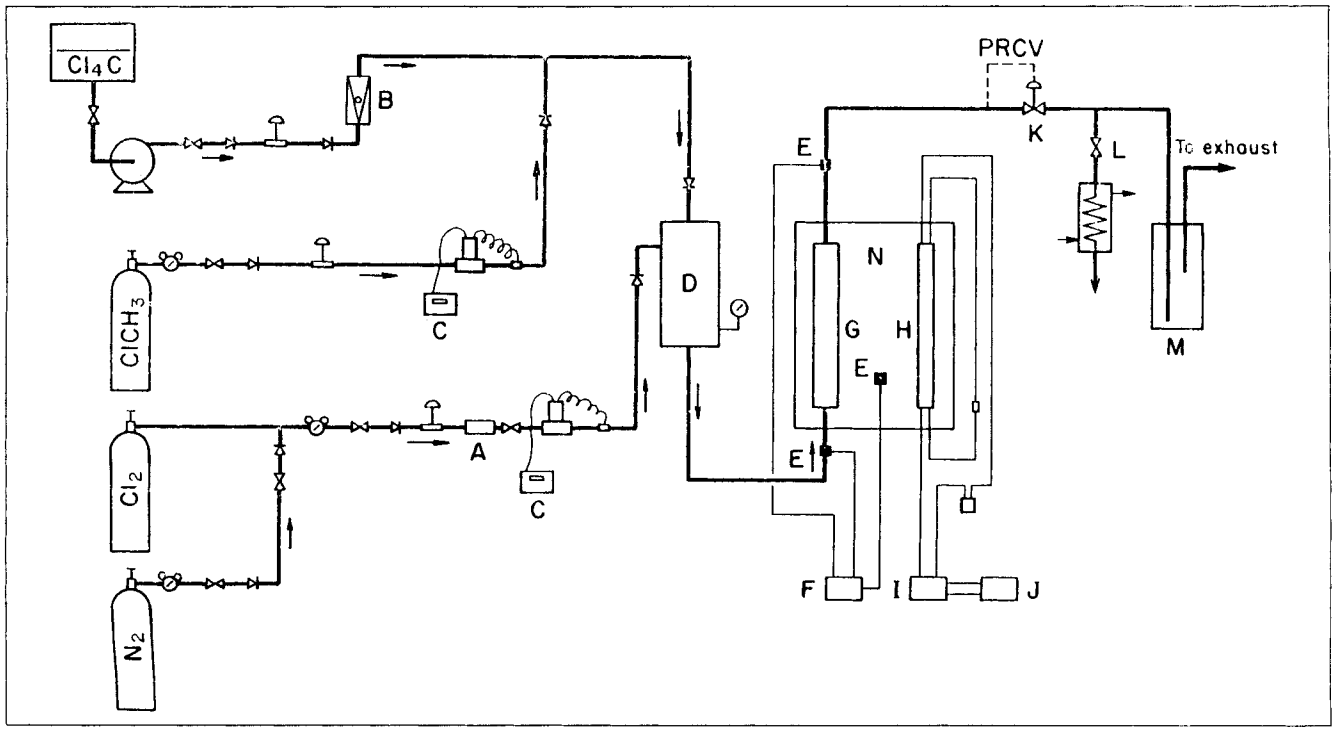

Figure 1. Experimental setup.

accounted for following the procedure proposed by Clariá et al. (1988).

Numerical solution

When the expression for the LVREA is substituted into the equations representing the reaction rates, and in turn the obtained rates are substituted into the mass and thermal energy balances, a set of seven (six mass balances and one thermal energy balance) partial integrodifferential equations must be solved. The solution can be obtained by finite difference techniques, using an implicit method with a relaxation coefficient equal to one (Cabrera et al., 1991a).

This method has been shown to be effective for the photochlorination of methane in the gas phase and under rather small chlorine concentrations (no higher than 0.006 mol/L). In the liquid-phase case, the solubility of chlorine in carbon tetrachloride is very high. According to the data of Linke (1958), at 19°C the chlorine solubility is 2.05 mol/(L × chlorine pressure in atm). At 450 kPa of total pressure, even under mild reaction conditions (excess of carbon tetrachloride), the amount of chlorine present is sufficiently high to turn the optical thickness of the reaction medium very thick. Under these conditions, an important fraction of the incoming light will be absorbed in a very thin layer close to the reactor wall. Then, strong reaction will occur in this zone and very steep changes in concentration will be present. A nonuniform integration grid in the radial direction was necessary.

As a result of a different phenomenon, a similar reasoning was needed in the axial direction. In fact, the incoming concentrations in the liquid phase are several orders of magnitude greater than those prevailing in the gas phase. Under these conditions, the rate of reaction is very intense. A strong change in chlorine concentration occurs in the first portions of the reactor length. A nonuniform grid in the axial direction was also used.

Variables were changed according to the suggestions of Agrawal and Peckover (1980). The dimensionless radial coordinate was changed according to:

$$\gamma = f(\xi) = \frac{\tanh(\xi \tanh^{-1}\sqrt{1-\delta_r})}{\sqrt{1-\delta_r}} \tag{15}$$

and for the dimensionless axial coordinate, the following transformation was used:

$$\eta = g(\zeta) = 1 - \frac{\tanh[(1-\zeta)\tanh^{-1}\sqrt{1-\delta_z}]}{\sqrt{1-\delta_z}} \tag{16}$$

In Eqs. 15 and 16, δ is a normalized boundary layer thickness which has to be chosen according to the physics of the problem. A value of $\delta_r = \delta_z = \delta = 0.1$ was found to produce satisfactory results. The function defined by Eq. 15 accumulates points in the radial integration grid close to the reactor wall, while that defined by Eq. 16 produces a similar effect in the axial integration grid at the reactor entrance. These functions were substituted into Eqs. 10 to 14, and the proper numerical method performed afterward.

The three-dimensional nature of the radiation field was incorporated into the two-dimensional mass and energy balances following the method proposed by Romero et al. (1983). The coupling of the attentuation of radiation with the reaction extent was solved by superimposing an iterative procedure on the finite difference solution, according to the method described by Cassano et al. (1986).

Experiments

Setup

It was necessary to make important changes to the equipment used in previous works for photochlorinations in the gas phase. Working with flammable and toxic reagents and products under pressure in a reactor made of quartz requires special safety measures. Thus, the equipment was set up in a closed metallic cabin (2.80 m × 1.15 m × 2.20 m), with one swinging wall. In one of the fixed walls, an exhaust fan (100 m^3/min) was installed; in the front wall, a sliding door permitted the operator eventual access to the experimental setup. All the fluid circulating tubes were made of Teflon tubing sleeved with brass tubing. The equipment was operated from outside the closed cabin. An emergency system made with solenoid valves allowed the shutdown of a run from outside the cabin in a few seconds. Figure 1 shows the experimental apparatus.

The feed contained:

- Chlorine: Matheson, H.P. grade, 99.5%. The cylinder was vented to eliminate any noncondensable gases (Bernstein and Albright, 1972). The gas stream was passed through a 3-Å molecular sieve adsorber (A). The chlorine flow rate was measured with a Matheson mass flowmeter calibrated properly (C).
- Methyl chloride: Air Products, H.P. grade, 99.5%. The methyl chloride flow rate was measured with a Matheson mass flowmeter also calibrated previously (C).
- Carbon tetrachloride: Cicarelli, "pro-analysis" grade. It was purified before use with a Sartorious filter using a cellulose nitrate membrane of 0.2 microns. It was deoxigenated carefully by passing nitrogen gas through the liquid. It was fed at the desired pressure with a gear pump, Micropump type, from Cole-Parmer, and measured with a calibrated Gilmont ball flowmeter (B).

A mixer (D) filled with Teflon shavings was used to ensure a single-phase system, taking advantage of the very high solubility of methyl chloride and chlorine in the liquid carbon tetrachloride.

The tubular reactor (G) was made of quartz, heavy-wall tubing, Suprasil quality, and its dimensions are as shown in Table 4. Since the reactor tube must be cleaned very often and positioning at the focal axis of the ellipse is very critical, a special device was constructed that consisted of a holding support having three arms controlled by micrometric screws, symmetrically separated 120 degrees from each other. The inlet and outlet reactor temperatures were read as indicated by (F) with the aid of resistor thermometers (E).

Table 4. Photoreactor, Reflector and Lamp Characteristics

Parameter	Values
Reactor Dimensions	
Inside Diameter	$D_{in} = 3.10^{-3}$ m
Outside Diameter	$D_{ou} = 8.10^{-3}$ m
Length	$L_R = 0.30$ m
Reflector Dimensions	
Height	$L_{Rf} = 0.59$ m
Ellipse Major Axis	$2a = 1.07$ m
Ellipse Eccentricity	$e = 0.4$
TLK40/09 N Philips Lamp	
Nominal Power	$Pc = 40$ W
Diameter	$D_L = 0.038$ m
Arc Length	$L_L = 0.565$ m

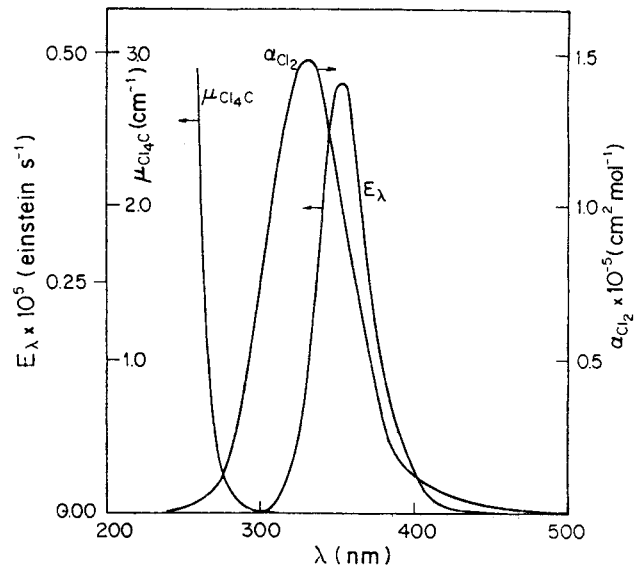

Figure 2. Chlorine absorptivities, spectral distribution of the lamp output power, and carbon tetrachloride absorption coefficient as a function of wavelength.

Based on Naperian logarithm.

A tubular, fluorescent-type, Philips lamp (H), of 40-W nominal output power was used. Its main characteristics are described in Table 4. This lamp was chosen, because the spectral distribution of its output power overlaps adequately with the chlorine molar absorptivity spectral distribution (Figure 2). A system similar to the one for the reactor was used for positioning of the lamp. To ensure the proper functioning of the lamp at the rated conditions, the operating input current, voltage and power were continuously monitored as indicated by (I) and (J) in Figure 1. The lamp was installed after a minimum of 100 hours of operation to ensure its use during the most stable period of its average lifetime.

The elliptical reflector (N) was made of aluminum sheet, specularly finished with Alzac treatment. It was constructed with less than 0.05-cm tolerance, and its main dimensions are as indicated in Table 4. The temperature inside the elliptical reflector space was measured as indicated by (E) and (F).

A pressure regulating control valve (PRCV), (K), (Mity-Mite back-pressure type from Grove Valve and Regulator Company) controlled the operating pressure. The regulator was modified to have all the parts in contact with the reacting fluid made of Teflon. The pressure regulator was also used to reduce the product stream pressure from 450 kPa to the atmospheric pressure existing in the sampling section.

Sampling was made of the sampling device (L). Afterward the outgoing liquid was bubbled through a concentrated solution of sodium hydroxide (M), before venting to the exhausting system. Details of the sampling procedure, which was very critical, are discussed in the next section.

All parts in contact with chlorine or the reacting mixture were made of quartz, Teflon, or Monel metal. Teflon and Monel Swagelock fittings were used in all connections. Teflon or Monel valves were used to adjust the flow rates.

Nitrogen gas (99.998%) was used to flush the whole reacting system after each run was finished to permit cleaning and maintenance routines.

Procedure

A checklist of routine procedures was established to verify the proper functioning of the whole reacting system before starting every run. It included a pressure test at about 800 kPa. The system was then flushed with nitrogen to eliminate oxygen and moisture. First, chlorine was fed to the system. Later, carbon tetrachloride and methyl chloride were added and mixed with chlorine in the mixer (D). The flow rates and pressures were properly adjusted, and a stabilizing period of 1.5 hours was allowed to achieve the steady-state conditions in pressure, flow rates, output concentrations, and temperatures. The steady-state operation under dark conditions was verified by analyzing samples of the outgoing stream every 10 minutes. When it was achieved, the lamp was turned on, and again a waiting period of 1.5 hours was allowed to obtain stable conditions particularly in lamp operation, flow rates, pressure, temperatures, and output product concentrations. At this stage, samples also were taken every 10 minutes. At steady state the lamp was shut off. Finally, all the feed supplies were stopped, and the whole system was flushed with nitrogen gas. Every experimental point was always subjected to a triplicate analysis.

Sampling was performed as follows. The product stream passed through a glass heat exchanger where it was cooled to $-10°C$ to minimize the loss of the dissolved gases (by flashing) when the pressure was reduced. Then, it was collected in an aqueous solution of potassium iodine during a specified amount of time. After complete absorption of chlorine (which liberated molecular iodine that remained in the water solution) and hydrogen chloride (which also remained dissolved in the aqueous medium), the organic phase was separated. Feed and unconverted chlorine were obtained by volumetric titration of the existing iodine in the aqueous solution, and chlorinated hydrocarbons (methyl chloride, methylene chloride, chloroform, and carbon tetrachloride) were analyzed by gas chromatography. Porapak Q-S (80/100 mesh), 200-cm-long columns were used, and the absolute values of concentrations were obtained after calibration of the detector system. Ethyl alcohol was used as an internal standard. Each gas chromatography analysis took approximately 10 minutes with the developed temperature program. The excess of carbon tetrachloride used as a solvent precluded an accurate measurement of that produced in the reaction, which was in any event generated in a very small quantity (this finding was later on corroborated by the theoretical simulations). The experimental mass balance could be closed within 4% in all the runs.

Table 5. Operating Conditions

Operating Variables	Units	Values
$Cl_2/ClCH_3$ Ratio in the Feed (F)	—	0.1–0.9
Methyl Chloride Initial Conc. ($C^o_{ClCH_3}$)	mol/L	0.62
Chlorine Initial Conc. ($C^o_{Cl_2}$)	mol/L	0.062–0.56
Carbon Tetrachloride Initial Conc. ($C^o_{Cl_4C}$)	mol/L	9.73–9.97
Inlet Reactor Temp. ($T°$)	K	291
Temp. of Air Surrounding Reactor (T_e)	K	293
Pressure	kPa	450
Volumetric Flow Rate (Q)	m^3/s	$2.5\ 10^{-5}$
Reynolds Number (Re)	—	330

After each run was completed and the system was flushed with nitrogen, the reactor was cleaned according to the following routine: 1) potassium hydroxide alcoholic solution; 2) hydrochloric acid aqueous solution; 3) distilled water; 4) reagent-grade absolute ethyl alcohol; 5) reagent-grade acetone; and 6) reagent-grade petroleum benzine (boiling point 60–80°C).

Table 5 shows a compedium of the operating conditions used in this work. It should be noted that during the whole experimental program chlorine and methyl chloride were always dissolved in the liquid carbon tetrachloride forming a homogeneous solution.

The experimental results were calculated as follows.

Methyl chloride conversion:

$$X_1 = \frac{\sum_{j=2}^{3} C_j}{C_1 + \sum_{j=2}^{3} C_j} \tag{17}$$

Chlorine conversion:

$$X_5 = 1 - \frac{C_5}{C_5^0} \tag{18}$$

Product selectivities:

$$S_i = \frac{C_i}{\sum_{j=2}^{3} C_j} \quad i = 2, 3 \tag{19}$$

In Eqs. 17 and 19, carbon tetrachloride production has been ignored. It could not be detected in the experiments, and the theoretical simulation confirmed that within the experimental accuracy, this assumption was correct.

Results

System parameters for a priori predictions

Computer predictions obtained from the numerical solution of the four balances require the evaluation of different transport and thermodynamic properties. They were obtained as follows:

- *Density* of the mixture was calculated as a linear combination of the densities of pure components (Raznjevic, 1976).
- *Viscosity* for each pure component was obtained from Yaws (1977); the mixture viscosity was computed according to Reid et al. (1977).
- *Diffusivities*, with the assumption of pseudobinary systems (large excess of carbon tetrachloride), were calculated using the Wilke and Chang correlation (Reid et al., 1977).

Table 6. Values of the Kinetic Constants

Steps	Log A	E (J·mol^{-1})
2	14.175*	12,322
2′	12.1*	34,309
3	11.971*	12,242
3′	14.0*	89,538
4	13.996*	12,475
4′	12.0*	46,861
5	12.291*	17,342
5′	14.0*	87,864
6	13.739*	13,411
6′	11.8*	56,066
7	12.285*	25,089
7′	14.3*	79,078
8	13.680*	—
9	13.680*	—
10	13.680*	—
11	14.345**	−7,029

* $cm^3 \cdot mol^{-1} \cdot s^{-1}$
** $cm^6 \cdot mol^{-2} \cdot s^{-1}$

• *Heat capacity* of the mixture was obtained from pure-component heat capacities according to Yaws (1977).

• *Conductivity* of the mixture was calculated with the Li correlation (Reid et al., 1977).

• *Quartz conductivity* was obtained from Perry and Chilton (1973).

• *Heat transfer coefficient* between the reactor wall and the still air surrounding the reactor was obtained with the Kato et al. correlation for natural convection outside tubes (Perry and Chilton, 1973).

• *Reaction heat* for each one of the global reactions R1, R2 and R3 was calculated from the heat of formation of pure components according to Reid et al. (1977).

• *Methyl chloride solubilities* in carbon tetrachloride were taken from Stephen and Stephen (1963), as a function of P and T.

• *Chlorine solubilities* in carbon tetrachloride were taken from Linke (1958) based on the data published by Taylor and Hildebrand (1923) and Smith (1955), as a function of P and T.

• *Chlorine radiation absorptivities* as a function of wavelength were taken from Gibson and Bayliss (1933).

• *Radiation output power and output power spectral distribution* were taken from the lamp manufacturer specifications (Philips, 1984).

• *Carbon tetrachloride radiation absorption coefficients* as a function of wavelength were taken from spectrophotometric measurements.

• *Quartz radiation transmission coefficient* was taken from Koller (1965).

• *Elliptical reflector reflectivities* as a function of wavelength were taken from Koller (1965).

• *Reaction kinetic constants* were taken from the results of Cabrera et al. (1991a), obtained in the photochlorination of methane in the gas phase. Since carbon tetrachloride is a non-polar solvent and all possible transport limitations are taken into account by the reactor model, these specific rate constants, based on the reaction mechanism, should be valid also for the liquid phase (Benson, 1960; Russell et al., 1963; Hill and Reiss, 1968). This includes also the primary quantum yield.

Radiation absorption properties of chlorine and carbon tetrachloride, as well as the emission characteristics of the lamp, shown in Figure 2 are specific and important to this work. The kinetic constants used in modeling the reaction kinetics are depicted in Table 6.

All these parameter values were taken into account or calculated for the reactor model. Consequently, no parameter adjustment was necessary. If the experimental results agree well with the theoretical predictions, the model clearly has achieved an *a priori* design of this photochemical process.

Computed vs. experimental results

Reactant conversions and product selectivities were calculated as follows:

$$X_i = 1 - \frac{\langle C_i \rangle}{\langle C_i^0 \rangle} \qquad i = 1, 5 \tag{20}$$

$$S_i = \frac{\langle C_i \rangle}{\sum_{j=2}^{4} \langle C_j \rangle} \qquad i = 2 \text{ to } 4 \tag{21}$$

where

$$\langle C_i \rangle = \frac{\int_A v_z(r) C_i(r, z) r \, dr \, d\beta}{\int_A v_z(r) r \, dr \, d\beta} \tag{22}$$

In Figures 3a and 3b, the theoretical predictions (solid line) and the experimental results are plotted for methyl chloride conversion and product (S_2 and S_3) selectivities as a function of the chlorine to methyl chloride ratio in the feed. Considering the difficulties in the prediction of the radiation field (lamp characteristics were those corresponding to nominal specifications) and the important number of deterministic parameters used in the modeling (taken from published results and correlations), one can say that the agreement is very good. Most discrepancies are attributed certainly to the difficulties associated with the sampling procedure; this problem was more critical at low conversions. However, an additional source of error should be mentioned; it was more important at high conversions. Temperature effects were incorporated only to the reaction-specific kinetics constants and not to the other physico-chemical properties of the reacting system. Since temperature rises as high as 40 K were observed, with a more elaborated model (and additional computation difficulties) this problem could have been taken into account. It is very likely that this simplification is also responsible for part of the differences.

In the range of concentrations and average residence times used in these experiments, methyl chloride conversion never exceeded 70%, but nearly 100% of chlorine conversion was achieved in all the runs. Disappearance of chlorine was observed visually (changes in the color of the reacting solution) from the 50% of the reactor-illuminated length onward.

Some runs (not reported here) were made with a value of F greater than 0.9 to ensure that chlorine be present along the whole reactor. The reaction rate, however, was so fast that a high temperature rise was observed and gaseous methyl chloride and chlorine began to separate from the liquid phase.

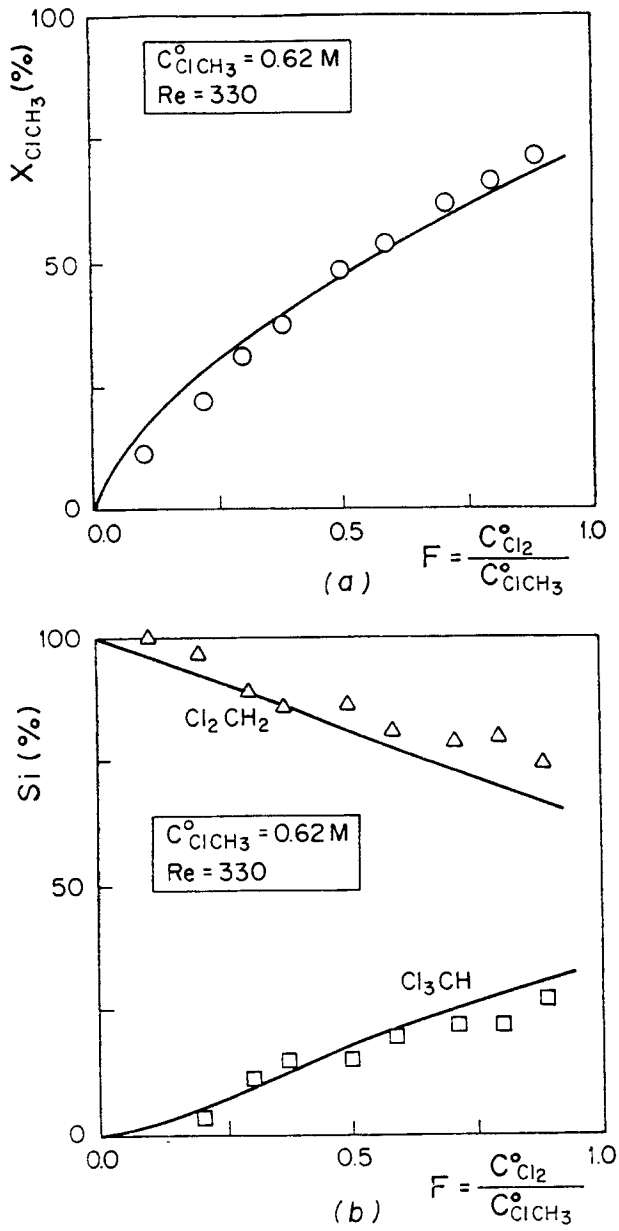

Figure 3. a. Methyl chloride conversion vs. feed molar ratio (chlorine/methyl chloride); b. Methylene chloride and chloroform selectivity vs. feed molar ratio.

Theoretical predictions are indicated by solid lines.

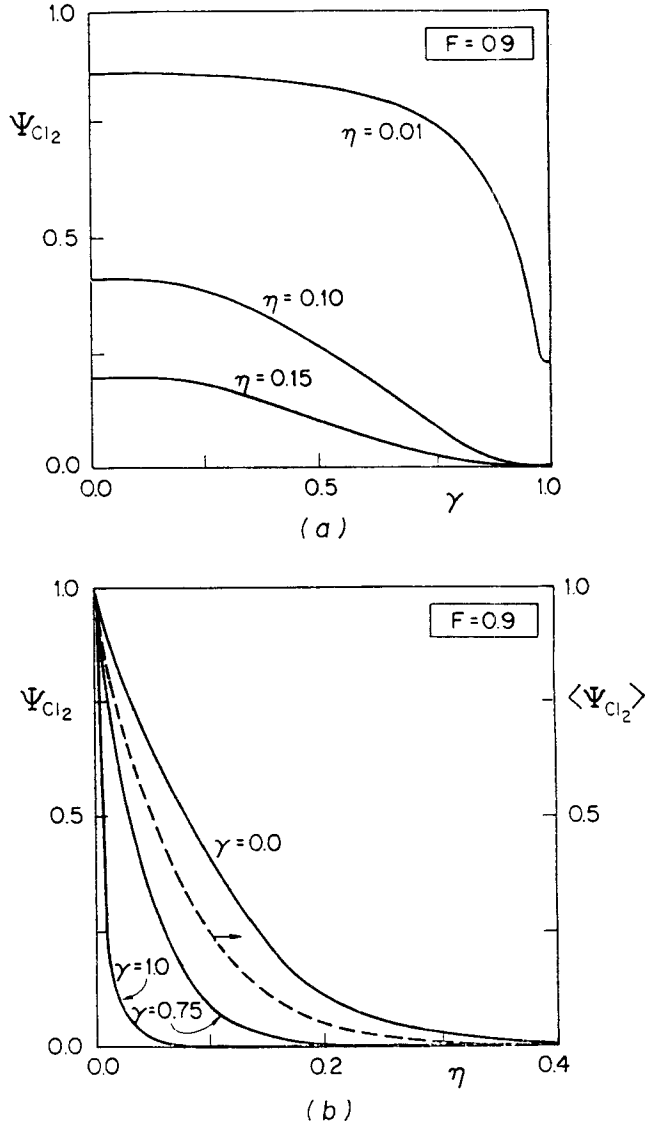

Figure 4. a. Dimensionless chlorine concentration vs. radial position (axial position is the parameter); b. dimensionless chlorine concentration vs. axial position (radial position is the parameter).

Both figures for $F = 0.9$.

Under these conditions, the reactor was no longer homogeneous and the system would have required a different form of sampling. Moreover, for a gas-liquid system (heterogeneous), this theoretical model cannot be applied. The available experimental setup did not allow a safe operation at higher pressures.

It is interesting to note that keeping the methyl chloride conversion rather low (at a F ratio of about 0.1) an almost 100% of methylene chloride selectivity can be achieved. Under our operating conditions, no maximum for the chloroform selectivity was obtained, and it is clear that the selectivity curve for $F = 1$ has not begun to level off yet. Theoretical predictions indicated that at this point the corresponding value for the carbon tetrachloride selectivity was about 3.5%.

Concentration profiles

Once the theoretical predictions were verified experimentally, one can proceed to use the complete reactor model to investigate performance of the reactor in more detail. The results for concentrations are shown in Figures 4a and 4b for $F = 0.9$.

Figure 4a represents the radial concentration profiles (axial position is the parameter). Note that at the feed conditions, the absorption coefficient for chlorine has a maximum value of 82 cm^{-1}. The chlorine concentration drastically drops in the regions close to the reactor wall, even at points located

immediately after the reactor entrance ($\eta = 0.01$). When 15% of the reactor has been traveled, the maximum chlorine concentration (at the reactor centerline) drops to about 20%. These results explain why the conventional (uniform grid) finite difference numerical method could not be used. Obviously, it is necessary to have a very refined integration mesh in the regions close to the reactor wall and to the reactor entrance. At the same time, these results indicate that when the reacting medium is optically thick, the combined effects produced by the strong reactant absorption in regions close to the reactor wall and the velocity profile distribution inside the reactor prevail over the radiation concentration effect produced by the elliptical reflector toward the reactor centerline and any possible effect of the radial diffusion of chlorine toward the reactor wall. (This could replenish the depleted chlorine concentration region.)

Clearly, a good reactor design for the liquid-phase operation with optically thick reacting media should be aimed at increasing as much as possible the radial mixing, with turbulent flow conditions, for example. This is a conclusion of general validity. Whenever the system has a very strong radiation absorption, mixing in the radiation characteristic direction (the radial one in this case) facilitates the operation and increases the yield. Working with simple models, this conclusion was demonstrated by Cassano and Alfano (1989) following the lines of a pioneering work done by Hill and Felder as early as 1965. Similar conclusions were obtained by André et al. (1982, 1983).

This reaction in the liquid phase is so fast that even under turbulent flow operation (by a substantial increase of the convective flow), the reactor would not need to be very long.

Figure 4b shows the axial concentration profiles using the radial position as a parameter (note that only 40% of the dimensionless axial coordinate has been plotted). The broken line indicates the cup averaged axial concentration profile. Clearly, at the reactor wall the chlorine concentration drops to almost zero in less than 10% of the reactor length and the cup-averaged concentration is almost zero when 40% of the reactor length has been reached. As mentioned earlier, the experimental results showed no detectable chlorine at the reactor outlet. These curves also show that the chlorine concentration always exhibits its maximum values along the reactor centerline. These considerations are important because the reactor temperature behavior shows a pattern that can be explained mostly on the basis of the changes in the chlorine concentration radial profiles.

These simulations demonstrate that 60% of the reactor was useless under the operating conditions employed. Obviously, even under mild operating conditions, the reaction in the liquid phase is very fast. These results clearly prove the importance of a validated rigorous model for design purposes. Evidently, simulations to produce the design under turbulent flow conditions, for example, could be performed with no additional difficulties.

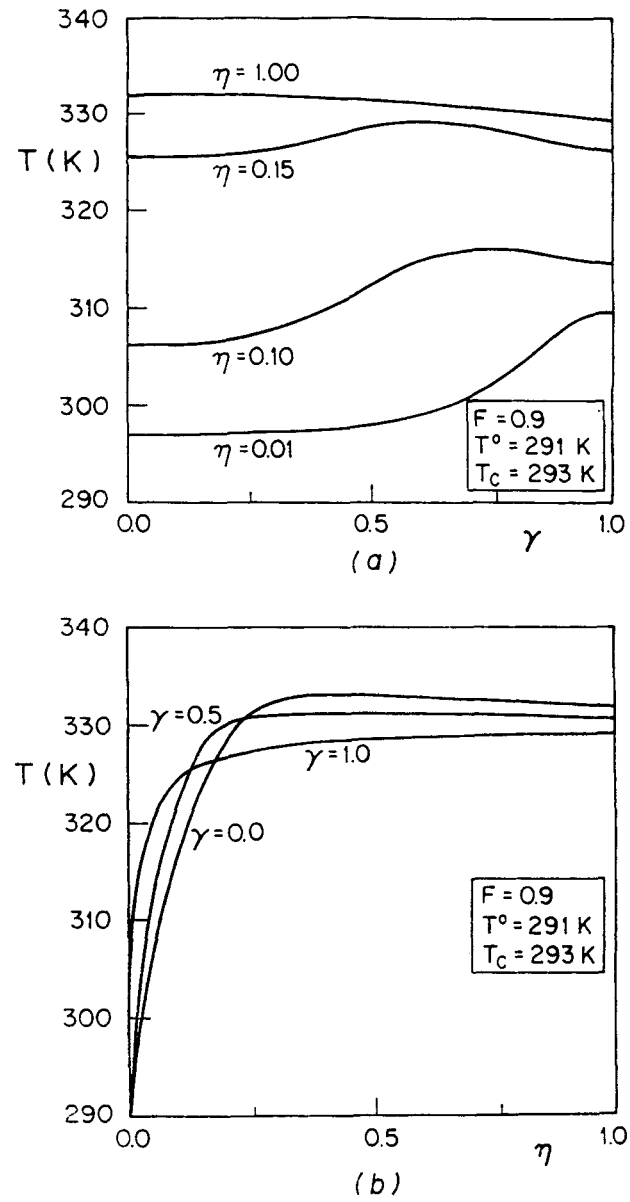

Figure 5. a. Dimensionless temperature vs. radial position (axial position is the parameter); b. dimensionless temperature vs. axial position (radial position is the parameter).

Both figures for $F = 0.9$.

Temperature profiles

A similar analysis can be done with the temperature profiles. The results are shown in Figures 5a and 5b, also for $F = 0.9$.

Figure 5a shows radial temperature profiles (axial position is the parameter). Initially, at $\eta = 0.01$, the maximum temperature is obtained at the reactor wall. This result is in agreement with the phenomenon observed with the chlorine concentration profiles. When the reactants progress along the reactor length, the temperature maximum moves toward the reactor centerline. It is the result of the combined effect of the displacement of the maximum reaction rate from the wall toward the center (once the controlling reactant has been depleted in the first region) and the heat transfer characteristics of the system.

At $\eta = 1.0$ (reactor outlet), the maximum of the radial temperature profile is at the center of the reactor, and the temperature gradient in passing from the reactor wall to the reactor centerline has diminished. This leveling of the temperature radial profile can be observed more clearly in the liquid-phase chlorination and does not occur to the same extent in the gas-

phase reactions, although it should be noted that in the latter the initial temperature gradients are less severe (Cabrera et al., 1991a). The difference is obviously caused by the disparity in heat transfer properties of both media. The initial temperature differences between the wall and the center of the reactor are much more pronounced in the liquid-phase reaction. Six associated causes explain this result:

1. Reaction rates are faster in the liquid phase because concentrations are higher.
2. At the beginning of the reactor, reaction occurs mainly in regions very close to the reactor wall due to the high radiation absorption characteristics of the liquid phase.
3. The velocity distribution in the laminar flow regime produces smaller fluid velocities in the regions close to the reactor wall (this phenomenon is more significant when the viscosity is higher in the liquid phase).
4. Radial heat conduction is not sufficiently high as to counterbalance the second and third effects.
5. Radiation concentration effect toward the reactor centerline produced by the elliptical reflector cannot overcome the second and third effects.
6. The radial diffusion of chlorine toward the depleted concentration region is slower in the liquid phase.

It can be concluded that an industrial design should be made in such a way that a strong increase in radial mixing could be obtained.

Figure 5b shows the axial temperature profiles using the radial position as a parameter. When the reactants reach approximately 13% of the reactor length, the highest temperature value has moved to a midway position between the reactor wall and the reactor center. For any position beyond the first 25% of the reactor length, this value is located at the reactor centerline. At the reactor outlet, differences between the wall and the center of the reactor have been reduced to the minimum value of those observed in the last 75% of the reactor length.

It is important to note that the theoretical predictions agree very well with the experimental measurements of the differences between the inlet and the outlet temperatures. In fact, for $F=0.9$, a 40-K temperature rise was experimentally observed.

Conclusions

The photochlorination of methyl chloride in the liquid phase and under moderate pressure has been modeled rigorously and verified experimentally. The main conclusions are:

- Experimental results agree well with the model predictions that were performed without using any empirically adjusted parameters.
- It was confirmed that using a nonpolar solvent, when the appropriate reactor model is applied, the specific kinetic constants obtained for the reaction mechanism in the gas phase can be used safely in the liquid phase and under moderate pressures.
- Operating conditions exist, in which a very high methylene chloride selectivity can be achieved.
- The very high optical density of the liquid system and the laminar flow regime generate strong concentration and temperature gradients inside the reactor.
- Due to the high radiation absorption in the regions of the reactor close to the reactor wall, the numerical solution of the model required the use of a modified mesh that concentrates the points of the radial grid toward the reactor wall. Similarly, due to the high reaction rates in the regions very close to the reactor inlet, a similar refined computational mesh had to be used in the axial direction.
- For the photochlorination of methyl chloride in industrial applications using tubular flow reactors turbulent flow operation is preferred to facilitate radial mixing from three different points of view: 1. more uniform radiation absorption; 2. more uniform concentration profiles; and 3. more uniform temperature profiles. These three improvements will enhance reactor operation safety and yields.

Acknowledgment

The authors are grateful to Mr. Antonio Negro for his participation in the experimental work. They are also grateful to Consejo Nacional de Investigaciones Científicas y Técnicas (CONICET) and Universidad Nacional de Litoral (U.N.L.) for their financial aid.

Notation

a = major semi-axis of the ellipse, m
A = area, m^2; preexponential factor, $m^3 \cdot mol^{-1} \cdot s^{-1}$ (except for reaction M-11 where the unit is $m^6 \cdot mol^{-2} \cdot s^{-1}$)
$\underset{\approx}{A}$ = propagation reaction array in Table 2, dimensionless
$\underset{\approx}{B}$ = stable species array in Table 2, dimensionless
C = concentration, $mol \cdot m^{-3}$
Cp = heat capacity, $J \cdot mol^{-1} \cdot K^{-1}$
D = diameter, m
$\mathfrak{D}_i$ = diffusion coefficient of species i, $m^2 \cdot s^{-1}$
e = ellipse eccentricity, dimensionless
e^a = volumetric rate of radiant energy absorption, einstein $\cdot m^{-3} \cdot s^{-1}$
E = radiant energy flow rate, einstein $\cdot s^{-1}$; activation energy, $J \cdot mol^{-1}$
F = feed molar ratio (chlorine/methyl chloride), dimensionless
$\underset{\approx}{g}$ = initiation reaction array in Table 2, dimensionless
G = incident radiation, einstein $\cdot s^{-1} \cdot m^{-2}$
Ge = r_R/L_R, geometrical number, dimensionless
h = heat transfer film coefficient, $W \cdot m^{-2} \cdot K^{-1}$
ΔH = heat of reaction, $J \cdot mol^{-1}$
I = specific intensity, einstein $\cdot s^{-1} \cdot m^{-2} \cdot sr^{-1}$
J = $\Phi\, e^a\, L_R/\langle v_z \rangle C_5^0$, dimensionless initiation rate
k = kinetic constant, $m^3 \cdot mol^{-1} \cdot s^{-1}$ (except for reaction M-11, where the unit is $m^6 \cdot mol^{-2} \cdot s^{-1}$)
K = $k\, C_5^0\, L_R/\langle v_z \rangle$, dimensionless kinetic constant (for $i=11$, $k\, (C_5^0)^2\, L_R/\langle v_z \rangle$)
L = length, m
Nu = $h_c\, D/\lambda$, Nusselt number, dimensionless
P = pressure, Pa
Pc = lamp power consumption, W
Pe_i = $\langle v_z \rangle r_R/\mathfrak{D}_{im}$, mass Peclet number of species i, dimensionless
Pe_t = $Cp\langle v_z \rangle r_R/\lambda_m$, thermal Peclet number, dimensionless
Q = dimensionless heat of reaction; volumetric flow rate, $m^3 \cdot s^{-1}$
r = radial coordinate, m
R = reaction rate, $mol \cdot m^{-3} \cdot s^{-1}$
$\underset{\approx}{R}$ = intermediate species concentration array in Table 2, dimensionless
Re = $D\, \langle v_z \rangle\, \rho/\mu$, Reynolds number, dimensionless
S_i = selectivity of product i, dimensionless
T = temperature, K
$\underset{\approx}{T}$ = termination constant array in Table 2, dimensionless
$U(\gamma)$ = $v_z(r)/\langle v_z \rangle$, dimensionless velocity
v = velocity, $m \cdot s^{-1}$
X_i = conversion of species i, dimensionless
z = cylindrical coordinate, m

Greek letters

α = molar absorptivity, $m^2 \cdot mol^{-1}$

β = cylindrical coordinate, rad
γ = r/r_R, dimensionless radial coordinate
Γ = reflection coefficient, dimensionless
δ = normalized boundary layer thickness, dimensionless
ζ = axial coordinate in transformed space, dimensionless
η = z/L_R, dimensionless axial coordinate
θ = spherical coordinate, rad
κ = value in Table 3
λ = wavelength, nm; thermal conductivity, $W \cdot m^{-1} \cdot K^{-1}$
μ = absorption coefficient, m^{-1}; viscosity, $kg \cdot m^{-1} \cdot s^{-1}$
ν = frequency, s^{-1}
ξ = radial coordinate in the transformed space, dimensionless
ρ = spherical coordinate, m; density of the reacting mixture, $kg \cdot m^{-3}$
τ = $(T-T^0)/(T_c-T^0)$, dimensionless temperature
Υ = transmittance, dimensionless
ϕ = spherical coordinate, rad
Φ = quantum yield, $mol \cdot einstein^{-1}$
Ψ_i = C_i/C_5^0, dimensionless concentration
Ω = solid angle, sr
Ω_i = $R_i L_R/\langle v_z \rangle C_5^0$, dimensionless reaction rate of species i

Subscripts

c = heat exchange fluid surrounding the reactor
i = relative to species i
I = reception point or property of the incident ray
in = reactor internal wall
init = relative to the initiation step
L = property of the lamp
m = property of the reacting mixture
0 = relative to the surface of radiation entrance
ou = reactor external wall
p = relative to propagation step
r = relative to radial coordinate
R = reactor property
Rf = reflector property
t = relative to termination step
z = relative to z coordinate
ν = dependence on frequency
1 = integration lower limit
2 = integration upper limit

Superscripts

(k) = relative to overall reaction k
0 = inlet conditions
$'$ = reverse reaction
$*$ = relative to attenuation trajectory

Special symbols

$\langle\ \rangle$ = average value
Δ = interval
$\hat{}$ = free radical

Literature Cited

André, J. C., A. Tournier, M. Niclause, and X. Deglise, "Industrial Photochemistry: II. Influence of the Stirring of Unstable Radical Species on the Kinetics of Consecutive Long-Chain Photochemical Reactions," *J. of Photochemistry*, **18**, 57 (1982).

André, J. C., A. Tournier, and X. Deglise, "Industrial Photochemistry: III. Influence of the Stirring of Reactants on the Kinetics and Selectivity of Consecutive Long-Chain Photochemical Reactions," *J. of Photochemistry*, **22**, 7 (1983).

Agrawal, A. K., and R. S. Peckover, "Nonuniform Grid Generation for Boundary-Layer Problems," *Comp. Phys. Comm.*, **19**, 171 (1980).

Akiyama, S., T. Hisamoto, T. Takada, and S. Mochizuki, "Catalytic Conversions of Methanol to Chloromethanes," *J. Catal. Convers. Synth. Gas Alcohols Chem.*, p. 419, R. G. Herman, ed., Plenum, New York (1984).

Baginski, F. C., "Photochemical Reaction of Hydrogen Sulfide with n-Octene-1," PhD Diss., Yale Univ., New Haven, CT (1951).

Benson, S. W., *The Foundations of Chemical Kinetics*, McGraw-Hill, New York (1960).

Bernstein, L. S., and L. F. Albright, "Kinetics of Slow Thermal Chlorination of Hydrogen in Nickel Tubular Flow Reactors," *AIChE J.*, **18**, 141 (1972).

Boynton, H. G., E. W. Lewis, and A. T. Watson, "A High-Pressure Photochemical Reactor," *Ind. Eng. Chem.*, **51**, 267 (1959).

Braun, A. M., M. T. Maurette, and E. Oliveros, German Patent 657978 of 1938 by I. G. Farbenindustrie, quoted in *Technologie Photochimique*, Presses Polytechniques Romandes, Lausanne (1986).

Braun, A. M., M. T. Maurette, and E. Oliveros, Japanese patent 82142927 of 1982 by A. Glass quoted in *Technologie Photochimique*, Presses Polytechniques Romandes, Lausanne (1986).

Cabrera, M. I., O. M. Alfano, and A. E. Cassano, "Selectivity Studies in the Photochlorination of Methane: I. Reactor Model and Kinetic Studies in a Non-Isothermal, Polychromatic Environment," accepted for publication in *Chem. Eng. Commun.* (1991a).

Cabrera, M. I., O. M. Alfano, and A. E. Cassano, "Selectivity Studies in the Photochlorination of Methane: II. Effect of the Radiation Source Output Power and Output Spectral Distribution," accepted for publication in *Chem. Eng. Commun.* (1991b).

Calvert, J. C., and J. N. Pitts, *Photochemistry*, Wiley, New York (1966).

Cassano, A. E., O. M. Alfano, and R. L. Romero, "Photoreactor Engineering: Analysis and Design," *Concepts and Design of Chemical Reactors*, Chap. 8, p. 339, S. Whitaker and A. E. Cassano, eds., Gordon and Breach, New York (1986).

Cassano, A. E., and O. M. Alfano, "Photoreactor Design," *Handbook of Heat and Mass Transfer: 3. Catalysis, Kinetics and Reactor Design*, Chap. 16, p. 583, N. P. Cheremisinoff, ed., Gulf Publishing, Houston (1989).

Cerdá, J., H. A. Irazoqui, and A. E. Cassano, "Radiation Fields Inside an Elliptical Photoreflector with a Source of Finite Spatial Dimensions," *AIChE J.*, **19**, 963 (1973).

Cerdá, J., J. L. Marchetti, and A. E. Cassano, "Radiation Efficiencies in Elliptical Photoreactors," *Lat. Amer. J. Heat Mass Transfer*, **1**, 33 (1977).

Chiltz, G., P. Goldfinger, G. Huybrechts, G. Martens, and G. Verbeke, "Atomic Chlorination of Simple Hydrocarbon Derivatives in the Gas Phase," *Chem. Rev.*, **63**, 355 (1963).

Clariá, M. A., H. A. Irazoqui, and A. E. Cassano, "*A Priori* Design of a Photoreactor for the Chlorination of Ethane," *AIChE J.*, **34**, 366 (1988).

De Bernardez, E. R., and A. E. Cassano, "Azimuthal Asymmetries in Tubular Photoreactors," *Lat. Amer. J. Heat Mass Transfer*, **6**, 333 (1982).

De Bernardez, E. R., and A. E. Cassano, "Methodology for an Optimal Design of a Photoreactor: Application to Methane Chloroderivatives Production," *Ind. Eng. Chem. Process Des. Dev.*, **25**, 601 (1986).

De Bernardez, E. R., M. A. Clariá, and A. E. Cassano, "Analysis and Design of Photoreactors," *Chemical Reaction and Reactor Engineering*, Chap. 13, p. 839, J. J. Carberry and A. Varma, eds., Marcel Dekker, New York (1987).

Gibson, G. E., and N. S. Bayliss, "Variation with Temperature of the Continuous Absorption Spectrum of Diatomic Molecules: I. Experimental—the Absorption Spectrum of Chlorine," *Phys. Rev.*, **44**, 188 (1933).

Hill, F. B., and R. M. Felder, "Effects of Mixing on Chain Reactions in Isothermal Photoreactors," *AIChE J.*, **11**, 873 (1965).

Hill, F. B., and N. Reiss, "Nonuniform Initiation of Photoreactions: II. Diffusion of Reactive Intermediates," *Can. J. Chem. Eng.*, **46**, 124 (1968).

Hirschkind, W., "Chlorination of Saturated Hydrocarbons," *Ind. Eng. Chem.*, **41**, 2749 (1949).

Holbrook, M. T., and T. E. Morris, "Liquid-Phase Chlorination of Chlorinated Methanes," U.S. Patent 4614572A (1986).

Irazoqui, H. A., J. Cerdá, and A. E. Cassano, "Radiation Profiles in an Empty Annular Photoreactor with a Source of Finite Spatial Dimensions," *AIChE J.*, **19**, 460 (1973).

Koller, L. R., *Ultraviolet Radiation*, 2nd ed., Wiley, New York (1965).

Linke, W. F., *Solubilities of Inorganic and Metal Organic Compounds*, Vol. 1, 4th ed., ACS, Washington, DC (1958).

Masini, J. J., "Procédé de Fabrication de Chlorométhanes Superieurs," European Patent 128818 A1 (1984).
McKetta, J. J., and W. Cunningham, *Encyclopedia of Chemical Processing and Design*, Vol. 8, Marcel Dekker, New York (1979).
Özisik, M. N., *Radiative Transfer and Interactions with Conduction and Convection*, Wiley, New York (1973).
Perry, R. H., and C. H. Chilton, *Chemical Engineers' Handbook*, 5th ed., McGraw-Hill Kogakusha, Tokyo (1973).
N. V. Philips Gloeilampenfabrieken, "Technical Bulletin: Lamps for Personal Care," Philips Lighting Div., The Netherlands, 1004 447 00021 (June, 1984).
Raznjevick, K., *Handbook of Thermodynamic Tables and Charts*, McGraw-Hill, New York (1976).
Reid, R. C., J. M. Prausnitz, and T. K. Sherwood, *The Properties of Gases and Liquids*, 3rd ed., McGraw-Hill, New York (1977).
Romero, R. L., O. M. Alfano, and A. E. Cassano, "Modelling and Parametric Sensitivity of an Annular Photoreactor with Complex Kinetics," *Chem. Eng. Sci.*, **38**, 1593 (1983).
Russell, G. A., A. Ito, and D. G. Hendry, "Solvent Effects in the Reactions of Free Radicals and Atoms: VIII. The Photochlorination of Aralkyl Hydrocarbons," *J. ACS*, **85**, 2976 (1963).
Santarelli, F., "One-Dimensional Radiative Transfer in Planar Participating Media," *Lat. Amer. J. Heat and Mass Transfer*, 7, 35 (1983).
Smith, T. L., *J. Phys. Chem.*, **59**, 188 (1955), quoted from W. F. Linke (1958).
Stephen, H., and T. Stephen, *Solubilities of Inorganic and Organic Compounds*, Vol. 1, Part 2/1, McMillan, New York (1963).
Taylor, N. W., and J. H. Hildebrand, *J. ACS*, **45**, 682 (1923), quoted from W. F. Linke (1958).
Tymoschuk, A. R., "Modelado de un Fotorreactor Multitubo 'Anular' con Pantalla Reflectora para una Reacción Homogénea Simple," Doctoral Diss., Universidad Nacional del Litoral, Santa Fe, Argentina (1990).
Yaws, C. L., *Physical Properties: a Guide to the Physical, Thermodynamic and Transport Property Data of Industrially Important Chemical Compounds*, McGraw-Hill, New York (1977).
Yokota, T., T. Iwano, and T. Tadaki, "Light Intensity in an Annular Photochemical Reactor," *Kagaku Kogaku Ronbunshu*, **2**, 298 (1976).

Manuscript received July 2, 1991.